Mon. Not. R. Astron. Soc. **337,** 103–108 (2002)

SLODAR: measuring optical turbulence altitude with a Shack–Hartmann wavefront sensor

R. W. Wilson★

Astronomical Instrumentation Group, Department of Physics, University of Durham, South Road, Durham DH1 3LE

Accepted 2002 July 10. Received 2002 July 5; in original form 2002 May 1

ABSTRACT

This paper discusses the use of Shack–Hartmann wavefront sensors to determine the vertical distribution of atmospheric optical turbulence above large telescopes. It is demonstrated that the turbulence altitude profile can be recovered reliably from time-averaged spatial cross-correlations of the local wavefront slopes for Shack–Hartmann observations of binary stars. The method, which is referred to as SLODAR, is analogous to the well known SCIDAR scintillation profiling technique, and a calibration against contemporaneous SCIDAR observations is shown. Hardware requirements are simplified relative to the scintillation method, and the number of suitable target objects is larger. The implementation of a Shack–Hartmann based turbulence monitor for use at the William Herschel Telescope is described. The system will be used to optimize adaptive optical observations at the telescope and to characterize anisoplanatic variations of the corrected point spread function.

Key words: atmospheric effects – instrumentation: adaptive optics – site testing – telescopes.

1 INTRODUCTION

Estimation of anisoplanatism is a key problem in the exploitation of adaptive optical (AO) correction for astronomy. Anisoplanatism is the variation of the atmospheric aberration of starlight, and hence the AO corrected point spread function (PSF), with field angle. Anisoplanatism changes in time with the continuously varying vertical distribution of optical turbulence [$C_n^2(h)$] above the telescope. Measurements of $C_n^2(h)$ are important for the design of new adaptive optical instruments and observations, for real-time optimization of AO systems and for the deconvolution of adaptively corrected images.

A knowledge of the statistical properties of $C_n^2(h)$ at the observing site is needed to predict the imaging performance and observable sky fraction for planned adaptive optical systems (Devaney & Keen 1998; Ellerbroek & Tyler 2001). For example, for a system which uses natural guide stars, the observable sky fraction for a given degree of correction will depend on the balance between the effects of anisoplanatism and photon starvation in wavefront sensing – brighter guide stars are on average found at greater angular distances from a target of scientific interest.

In a multi-conjugate adaptive optical system, the effects of anisoplanatism are reduced by deploying two or more deformable mirrors, placed at optical conjugates to the altitudes of the strongest turbulent layers. A measurement of the $C_n^2(h)$ profile is required to optimize the conjugation altitudes (Le Louarn et al. 2000).

★E-mail: R.W.Wilson@durham.ac.uk

The PSF for any AO system is field angle dependent due to anisoplanatism. Accurate deconvolution of AO corrected images therefore requires characterization of the PSF as a function of field angle. In a typical observation of an extended source few, if any, stellar point sources will be present in the field for use in PSF calibration. However the PSF can be estimated theoretically if a contemporaneous (or near contemporaneous) measure of the $C_n^2(h)$ profile is available (Fusco et al. 2000).

Two main methods have been employed for measurement of the $C_n^2(h)$ profile in recent years. Balloon-borne microthermal probes have been used to sample the turbulence strength and other atmospheric parameters with very high vertical resolution (Vernin & Muñoz–Tuñón 1994). However this is not a practical approach for regular monitoring or AO support observations.

The SCIDAR (SCIntillation Detection And Ranging) method has been very successfully exploited for several site characterization studies (Vernin & Muñoz–Tuñón 1994; Klückers et al. 1998; Avila, Vernin & Sánchez 2001). In this method, the turbulence altitude and wind velocity profiles are recovered from an analysis of the auto-correlation of scintillation patterns for bright binary stars, recorded in the pupil plane of a large telescope.

This paper discusses the use of an analogous binary star cross-correlation technique based on measurements of the local gradient of the wavefront phase aberration rather than the scintillation pattern. Since the method relies on measurements of wavefront slopes it is referred to as SLODAR (SLOpe Detection And Ranging). Although the altitude resolution of the method is limited by the achievable spatial sampling for the Shack–Hartmann sensor, it has advantages of cost and target availability relative to SCIDAR. The method can

be implemented with relatively inexpensive hardware to provide measurements of the turbulence profile in real-time .

Shack–Hartmann (or similar) studies of seeing-related parameters have been described previously. These include measurements of Fried's parameter, the spatial phase structure function, the outer scale of turbulence, angular anisoplanatism, and focal anisoplanatism (Dayton et al. 1992; Laurant et al. 1995; St-Jacques et al. 1997; Martin et al. 1998; Wilson et al. 1999). St-Jacques (1998) and Schöck & Spillar (1998) also describe measurements of turbulent layer velocities from Shack–Hartmann data via the temporal autocorrelation. This approach can be combined with the binary star method described here to estimate velocities as well as altitudes for individual turbulent layers (see Section 2).

The possibility of using Shack–Hartmann observations of binary stars to estimate turbulent layer heights has also been suggested by Welsh (1992), Bally et al. (1996) and St-Jacques (1998). The retrieval of optical turbulence parameters, including the vertical profile, from a statistical analysis of angle-of-arrival fluctuations for observations of the solar limb have been described by Irbah et al. (2001).

The details of the method for estimation of $C_n^2(h)$ are described in Section 2, and the results of detailed Monte Carlo simulations of the technique are presented. A comparison of simultaneous SCIDAR and (very low order) Shack–Hartmann turbulence profile measurements at the William Herschel Telescope (WHT), La Palma is presented in Section 4. Finally, the SLODAR turbulence profiler recently deployed at the WHT is described in Section 5.

2 METHOD

Consider a single turbulent layer at altitude H. A binary star with angular separation θ produces 'copies' of the aberrated wavefront at the ground, shifted by distance $S = H\theta$ with respect to one another. Hence there will be a peak in the (time averaged) spatial cross-correlation of the instantaneous aberration functions for the two stars, at baseline separation S in the direction of the binary separation.

Since we cannot observe the optical phase directly we must proceed via the measurement of related quantities. In the SCIDAR method short exposure images are recorded of the far-field scintillation pattern produced by the turbulence, for a binary star. Layer altitudes are inferred from peaks in the autocorrelation of the scintillation pattern. The strengths of the layers are determined via a fit to a theoretical expression for the covariance of scintillation intensity patterns (a function of layer strength and altitude).

Here in contrast we measure the local *gradient* of the phase aberration using a Shack–Hartmann wavefront sensor (WFS). A fully independent optical system could be used to observe each component of the binary. However a simpler setup uses a single lenslet array and large format detector. The binary star separations must then chosen so that the subaperture images do not merge – i.e. the spot patterns are either fully separated on the detector, or interleaved.

The spatial order $n_{\rm sub}$ of the wavefront sensor (number of subapertures across the telescope pupil) is limited by diffraction – subapertures must be at least 5–10 cm in diameter to allow measurement of centroid motions due to the seeing. The vertical resolution δH of the method is then related to the binary star separation angle θ by

$$\delta H = (D/n_{\rm sub})/\theta, \tag{1}$$

where D is the telescope aperture diameter, and assuming that the telescope pupil is sampled by exactly $n_{\rm sub}$ WFS lenslets across its diameter. The maximum sensing altitude is then

$$H_{\rm max} = n_{\rm sub}\delta H. \tag{2}$$

As an example configuration, consider a 20×20 subaperture lenslet array on the 4.2-m WHT. For a binary star with a separation of 50 arcsec, a maximum sampling altitude of approximately 17 km, with 850 m resolution, is then possible with the 4.2 m aperture. Larger binary separations will give improved sampling at the expense of lower maximum altitude. The maximum binary separation is set by the detector size or field of view of the optical system. The effective sampling of the profile for a given lenslet array could be increased by combining observations (in sequence) of two or more binary stars of different separations or by observing an asterism of three or more stars.

Centroids can be extracted from the Shack–Hartmann images in real time using modest computer hardware, so that image data need not be recorded. Calibration of the data and extraction of the $C_n^2(h)$ profile from the autocorrelation are straightforward and can be carried out in real time.

The following steps are required to retrieve the turbulence profile.

(i) Short exposure Shack–Hartmann images are recorded simultaneously for each star. Exposures must be short enough to 'freeze' the subaperture image motion (i.e. shorter than the crossing time for the fastest expected layer windspeed over the subaperture diameter).

(ii) Wavefront slopes are calculated for each subaperture in the two spot patterns, for each of the orthogonal 'tip' and 'tilt' directions. The mean slope over all illuminated subapertures is subtracted from the individual slopes for each star. This removes the effect of telescope tracking errors which are common to all subapertures.

(iii) The cross-correlation of the measured slopes is accumulated. If $s_{i,j}(t)$ is the slope in subaparture $(i,\ j)$ at time t, and $s'_{i,j}(t)$ the slope for the corresponding subaperture for the second star, we calculate

$$C(\delta i, \delta j) = \left\langle \sum_{i,j} s_{i,j}(t) s'_{i+\delta i, j+\delta j}(t)/O(\delta i, \delta j) \right\rangle, \tag{3}$$

where the angle brackets denote averaging over many independent WFS frames. Typically 1000 frames over 30 s are required. $O(\delta i, \delta j)$ is the number of overlapping subapertures (for which slope data are available) for separation $(\delta i, \delta j)$. The summation in equation (3) extends over the slopes measured for the both the tip and tilt directions.

(iv) Similarly the autocorrelation is estimated for a single star of the pair

$$A(\delta i, \delta j) = \left\langle \sum_{i,j} s_{i,j}(t) s_{i+\delta i, j+\delta j}(t)/O(\delta i, \delta j) \right\rangle. \tag{4}$$

$A(\delta i, \delta j)$ is effectively an estimate of the (altitude independent) 'impulse response' of the system to a single turbulent layer, and is used to recover the turbulence profile from $C(\delta i, \delta j)$ via a deconvolution. The normalized $C_n^2(h)$ profile is given by a one-dimensional cut through the deconvolved cross-correlation function in the direction of the binary star separation. If the telescope is equipped with a field rotator, the orientation of the binary can conveniently be aligned along the vertical or horizontal axis of the Shack–Hartmann array. Only the one-dimensional cross-correlation need then be calculated, i.e. in the δi or δj direction as appropriate.

(v) The total integrated turbulence strength can be found from the centroid data using, for example, the differential image motion method (Sarazin & Roddier 1990) or Zernike variance fitting (Wilson et al. 1999) as used here, to give a value for Fried's parameter r_0. The normalized turbulence profile can then be calibrated in terms of absolute $C_n^2(h)$ values.

In the absence of noise the normalized turbulence profile could be recovered from the cross-correlation and autocorrelation measurements via a straightforward deconvolution

$$C_n^2(h) \propto F^{-1}[F[C]/F[A]], \quad (5)$$

where F is the Fourier transform operator. In practice the correlation measurements are subject to noise which results from averaging over a finite number of atmospheric realizations in equations (3) and (4), and from shot noise in the WFS images. Hence the direct profile estimate from equation (5) is also noisy, typically evidenced by small (unphysical) negative $C_n^2(h)$ values and non-zero values at negative altitudes.

The number of free parameters in the profile estimate is relatively small [e.g. 16 discrete $C_n^2(h)$ values for a 16×16 WFS], so that a least-squares solution can be found rapidly via iterative minimization subject to the constraints of positivity and finite extent. Convergence to a unique solution has been found to be independent of the starting point of the fit, for both simulated and real data.

Rapid convergence can be obtained by using the direct solution of equation (5), with the constraints applied, as the starting point for the minimization. The chi-squared value for this constrained direct solution is typically less than a factor two greater than for the final least-squares solution. This indicates that the signal-to-noise ratio is high for correlation values averaged over approximately 30 s or more of centroid data in the high light level case.

For the SLODAR system at the WHT (Section 5), a continuously updating real-time display of the profile is provided using a 'leaky-box' average of correlation measurements over the previous few s. For purposes of speed, the constrained direct solution is used in this case.

In addition to altitudes and strengths, the wind velocities of individual turbulent layers can in principle be found from the tilt cross-correlation function calculated with a non-zero time delay δt between the centroid data streams for the two stars of the binary pair. Each peak in the two-dimensional autocorrelation function will then be shifted by a vector $\boldsymbol{v}(h)\delta t$ relative to its position for zero time delay. Here $\boldsymbol{v}(h)$ is the translational (wind) velocity for the layer at altitude h. In order to measure velocities, the Shack–Hartmann data must be recorded with a sampling interval small enough to track the wind motion – i.e. shorter than the crossing time for the wind velocity across the telescope aperture. The measurement of turbulence wind velocities from Shack–Hartmann data (without altitude determination) has been described elsewhere (Shöck & Spillar 1998; St-Jacques 1998) and is not pursued further here.

Hardware requirements for SLODAR are relaxed relative to SCIDAR. SCIDAR typically requires 1-cm resolution elements in order to adequately sample the scintillation pattern, and very short detector exposures ($\sim$1 ms) must be used. Since both the subaperture size and allowable exposure time for SLODAR are an order of magnitude larger, photon rates are much higher. An unintensfied detector with moderate read out noise characteristics can be used.

The higher spatial sampling of the pupil for SCIDAR does not necessarily yield greater vertical resolution of the turbulence profile. For SCIDAR this is limited to approximately 1 km by the Fresnel length associated with each turbulent layer (Klückers et al. 1998).

The small number of suitable target binary stars represents a significant restriction for SCIDAR as a turbulence monitor. Binaries with a combined visual magnitude of approximately 5 or greater, and a brightness differential of less than 1 mag are required. Hence there are significant periods when no suitable targets are available at high elevations. Much fainter stars can be used for SLODAR, and a larger magnitude differential can be tolerated – the requirement is simply that both stars must provide adequate SNR for centroid calculations – so that target objects are plentiful.

The problem of saturation of scintillation is also avoided with the SLODAR method. For strong turbulence, or when the scintillation is measured in a plane which is optically conjugate to an altitude which is very different from that of the turbulence, the relationship between turbulence strength and the amount of scintillation becomes non-linear. The layer strength may then be significantly under-estimated by SCIDAR.

3 MONTE CARLO SIMULATION

A detailed Monte Carlo simulation has been used to investigate the accuracy and limitations of $C_n^2(h)$ recovery from Shack–Hartmann data.

This was based on a general purpose adaptive optics simulation code developed at Durham, which is optimized for parallel execution and implemented on a dedicated Beowolf computing cluster. The code is written in the Numerical Python scripting language for ease of development. Optimized C-code accelerator modules are used for Poisson noise and certain other CPU-intensive calculations.

The simulation of turbulence profile measurements comprises the following components.

(i) Time evolving atmospheric turbulence model: made up of one or more phase screens with the von Karman spectrum of phase fluctuations, each with a specified coherence length [defining the fraction of $C_n^2(h)$ contributed by the layer], altitude and translational velocity. Propagation of starlight through the atmosphere is modelled via geometric ray tracing through the layers for any number of targets star at specified field angles.

(ii) Telescope: in this instance this simply serves to define the annular pupil function of the telescope.

(iii) Shack–Hartmann array: this is modelled as an array of square lenslets subdividing the telescope pupil. Each lenslet produces an image of the target star via a FFT of the atmospherically corrupted complex wave amplitude presented at the corresponding sub-section of the telescope pupil for a given time-step.

(iv) Detector: assumed to be a CCD camera with specified quantum efficiency and rms read-out noise level. Photon and detector read-out noise for a given target star brightness are modelled by replacing the high light level pixel values with random Poisson deviates at each model time-step.

(v) Centroider: centroids are derived from the low light level image, typically using a 4×4 pixel sub-region of the CCD for each subaperture image.

(vi) Correlator: this implements the data reduction steps described in Section 2 above to estimate the turbulence profile.

Simulations were performed to test the accuracy of the profile recovery as a function of the lenslet array sampling. Target star magnitude and magnitude differential limitations were also investigated.

Observations at the WHT were then modelled for 2 contrasting input atmospheric turbulence models, each comprising four turbulent layers, with the parameters shown in Table 1. Profile 1 represents a $C_n^2(h)$ which is relatively favourable for adaptive optics, with the bulk of the turbulence at close to ground level. Profile 2 is a more 'aggressive' profile, with a much larger contribution from high altitude layers, which would produce greater angular anisoplanatism. Each layer was given a wind velocity in the range 3 to 15 m s^{-1}. The input value of r_0 corresponding to the integrated turbulence strength was 15 cm in each case.

Table 1. Model input $C_n^2(h)$ profiles.

	Layer	Fractional $C_n^2(h)$	Altitude (m)
Profile 1	1	0.65	0.0
	2	0.20	2.0
	3	0.10	5.0
	4	0.05	10.0
Profile 2	1	0.35	0.0
	2	0.30	6.0
	3	0.20	9.5
	4	0.10	12.5

Measurementss using lenslet arrays with 8×8, 16×16 and 24×24 subapertures, observing a binary star of separation angle 40 arcsec, were modelled. Fig. 1 shows the measured cross-correlation and autocorrelation functions for the 24 × 24 WFS observing profile 2. The peaks corresponding to each of the four layers in the input $C_n^2(h)$ profile can be seen in the cross-correlation.

Fig. 2 shows example quantitative results for each simulation after 30 s integration with sampling interval 50 ms. For the 8 × 8 configuration the profile is sampled with 2.7 km resolution and layers are only clearly separated if their altitudes differ by 5.4 km or more. The 24 × 24 WFS gives 0.9 km resolution and all four layers in each profile are clearly resolved. Where individual layers are fully resolved in altitude, their relative strengths are recovered to within 10 per cent of their input values. The total integrated C_n^2, which is measured independently by the Zernike variance method, has an rms scatter of ±2 per cent about the input value.

For the 8 × 8 WFS the altitude resolution is too poor to give good reconstructions of the profiles, or even to identify the number of input layers. However profiles 1 and 2 are clearly distinguished, and the recovered profiles in fact provide an accurate measure of the degree of anisoplanatism for a conventional (natural guide star) adaptive optical system such as NAOMI. The values of isoplanatic angle (θ_0) calculated using the measured profiles for the 8 × 8 subaperture case differs by only 5 per cent from the values for the input profiles. This reduces to 1 per cent for the 24 × 24 WFS.

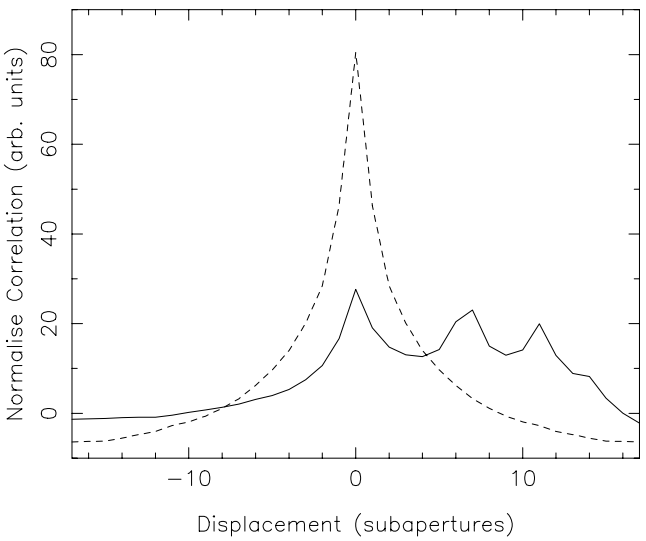

Figure 1. Cross-correlation (solid line) and autocorrelation (broken line) functions for simulated data (Profile 2, 24 × 24 subapertures – see text). Curves are one-dimensional slices through the two dimensional correlation functions in the direction of the binary star separation.

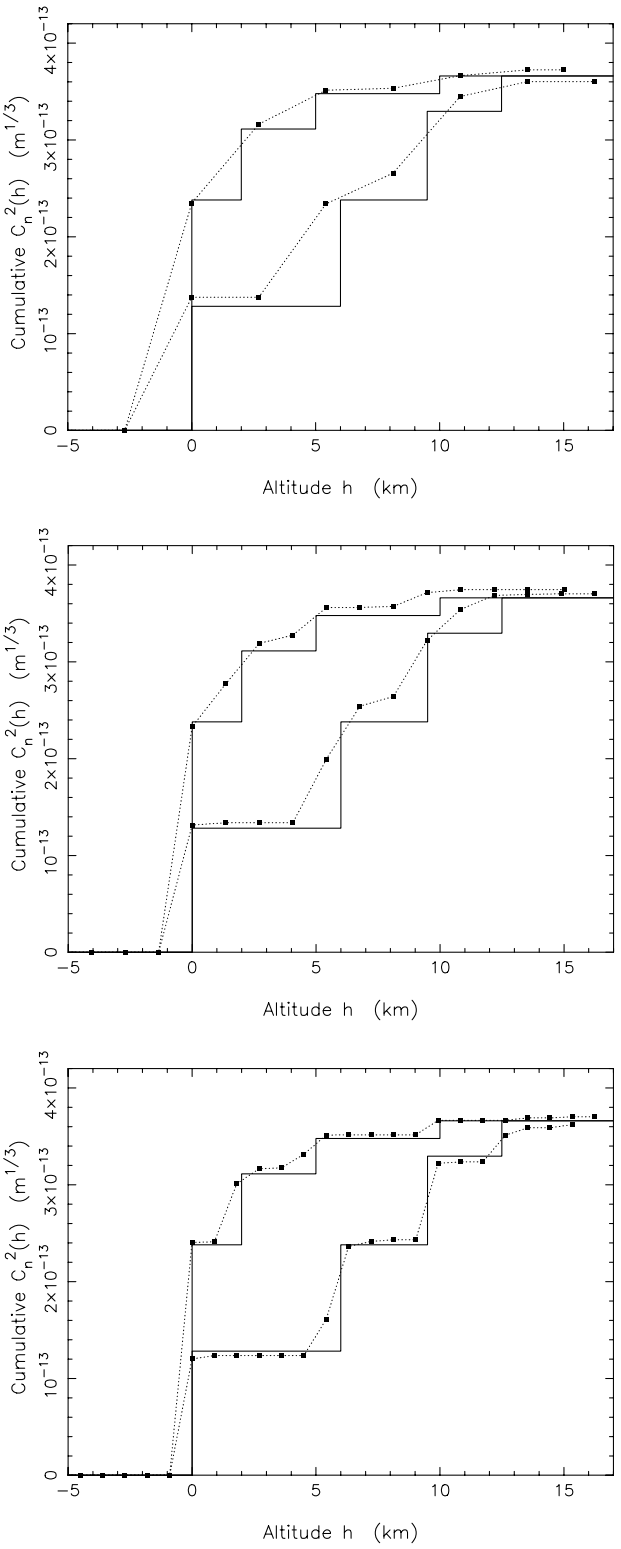

Figure 2. Example input (solid lines) and recovered (dotted lines) *cumulative* $C_n^2(h)$ distributions for the 2 simulated input profiles (see text). Top: 8 × 8 subapertures, middle: 16 × 16, bottom: 24 × 24 subapertures.

Centroiding noise is a function of photon noise and detector read noise, the image sampling in arcsec pixel^{-1} and the size of the CCD area used for centroiding. For these simulations a rms readout noise of 8 electron pixel^{-1}, and a quantum efficiency of 62 per cent in the

R-band were assumed. These values match the performance of the detector for the turbulence monitor to be installed at the WHT (see Section 5). A 4 × 4 pixel CCD subregion was used for centroiding each image, with an image sampling of 0.5 arcsec pixel^{-1}. Under these conditions a minimum of approximately 200 detected photons per subaperture per exposure was required. For higher photon rates the estimated turbulence profile did not differ significantly from the high light level case. For the case of a 24 × 24 subaperture Shack–Hartmann array at the WHT operating in the *R*-band, this implies a limiting magnitude of approximately $R = 9$, assuming 25 per cent total throughput to the WFS, including the CCD quantum efficiency.

The estimated profile was independent of the magnitude difference of the target stars, assuming that both stars were above the minimum brightness level. In practice the allowable brightness ratio will be limited by the dynamic range of the detector, but differences of 3 or more mags should be permissible for a typical CCD. In the low light level case, the zero offset value of the autocorrelation $A(0, 0)$ (but not the cross-correlation) will be biased by shot noise. Hence the brighter star of the target binary should always be used for calculation of the autocorrelation.

The effects of finite detector exposure time on the accuracy of the turbulence profile were investigated via the numerical simulation. The strength of a layer is significantly underestimated if the crossing time over a single subaperture of the WFS (i.e. subaperture diameter/layer wind velocity) is small compared to the exposure time. The fractional error in the layer strength was found to be less than 5 per cent for a layer with a crossing time equal to twice the exposure time. This increases to approximately 10 per cent for a faster moving layer with crossing time equal to the exposure time. Hence in practice the exposure time used should not be greater than one half of the crossing time for the fastest expected wind speed. Although ground-level windspeeds rarely exceed 20 m s^{-1}, velocities of 40 m s^{-1} or more can occur at high altitudes. Hence for a 16 × 16 subaperture WFS on the 4.2-m WHT (subaperture diameter 0.267 m), an exposure time of approximately 3 ms would be appropriate. A practical approach to optimization of the exposure time will be to measure (periodically) the layer velocities using very short exposure observations of a bright single star, via the spatio-temporal autocorrelation. The exposure time for SLODAR observations requiring (fainter) binary stars can then be set appropriately for the subaperture crossing time of the fastest detected windspeed.

4 OBSERVATIONS

A sequence of observations recorded at the 4.2-m WHT provide a calibration of the Shack–Hartmann method against the SCIDAR technique. A beamsplitter was used to divide the light from bright binary stars between a Shack–Hartmann sensor and the SCIDAR optics. The WFS comprised an 8 × 8 lenslet array (yielding 52 cm subapertures) coupled to a large format frame-transfer CCD which permitted frame rates of approximately 25 Hz, with exposure time 10 ms. The SCIDAR instrument has been described by Klückers et al. (1998). Scintillation patterns were recorded over a 1 m subsection of the telescope pupil, with 1 cm pixel^{-1} sampling, and an exposure time of approximately 1 ms. The original purpose of the observations was to correlate variations of anisoplanatism (measured with the WFS) with fluctuations of the turbulence profile determined from simultaneous SCIDAR observations. The results of that study will be presented separately.

The WFS data have very poor altitude resolution, since there were only 8 × 8 subapertures, and relatively narrow binary targets were used – typically 28 arcsec separation yielding 3.9 km resolution.

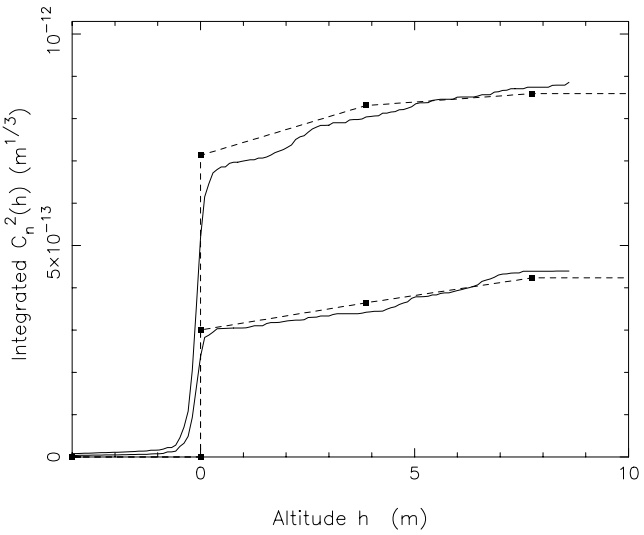

Figure 3. Example SCIDAR (solid lines) and Shack–Hartmann (broken lines) cumulative $C_n^2(h)$ profiles for 1998 June 11–12.

However a quantitative comparison of the $C_n^2(h)$ profiles is possible. Fig. 3 shows two examples of simultaneous SCIDAR and WFS measured profiles for 1998 June 11, recorded with an interval of 15 min. During this interval the (integrated) seeing improved from $r_0 = 9.1$ cm to $r_0 = 13.8$ cm. The $C_n^2(h)$ profiles show that this improvement was largely due to a factor two reduction in the strength of the ground level turbulence contribution. This is clear from both the SCIDAR and SLODAR profiles, which are in good agreement. Note that in this instance although the overall seeing improved markedly between the two observations, the isoplanatic angle θ_0 changed very little, since the ground layer does not contribute to anisoplanatism.

5 TURBULENCE MONITOR

A Shack–Hartmann based $C_n^2(h)$ monitor has been implemented for use at the WHT. The instrument will be used for site characterization studies and for optimization and calibration of observations with the NAOMI adaptive optical system.

The system is based on a QImaging 1350EX Firewire video camera which employs a 1360 × 1036 pixel CCD. The detector quantum efficiency is 62 per cent at 600 nm and readout noise is 8 electron pixel^{-1}. Frame rates of up to 60 Hz are possible for CCD sub-regions, with exposure times of 15 μs or greater.

Camera control and real-time data reduction are carried out on a single PC. Centroiding and cross-correlation calculations for each frame are performed during the subsequent CCD exposure and a display of the $C_n^2(h)$ estimate is continuously updated. The optical system comprises a lenslet array and reconfigurable collimating and re-imaging optics to define the subapertures across the WHT pupil.

6 CONCLUSION

It has been demonstrated that the vertical profile of optical turbulence can be recovered reliably from Shack–Hartmann wavefront sensor observations of binary stars. This SLODAR method has been verified by detailed Monte Carlo simulation and by comparison with contemporaneous SCIDAR observations.

The SLODAR technique can be implemented on any large telescope with relatively simple and inexpensive hardware and suitable

target binary stars are plentiful. Data reduction is straightforward and the turbulence profile can be recovered in real time.

ACKNOWLEDGMENTS

I am grateful to Nik Wooder, Florence Rigal, Chris Dainty and the Photonics group at Imperial College, London, for contributing the SCIDAR data used in this paper. Also to Richard Myers and Chris Saunter for useful discussions and comments.

The William Herschel Telescope is operated on the island of La Palma by the Isaac Newton group in the Spanish Observatorio del Roque de los Muchachos of the Instituto de Astrofísica de Canarias.

REFERENCES

Avila R., Vernin J., Sánchez L. J., 2001, A&A, 369, 364
Bally J., Theil D., Billawalla Y., Potter D., Loewenstein R. F., Mrozek F., Lloyd J. P., 1996, PASP, 13, 22
Dayton D., Pierson R., Spielbusch B., Gonglewski J., 1992, in Proc. ESO conf. on High Resolution Imaging by Interferometry II. ESO, Garching bei Munchen, p. 1047
Devaney N., Keen J., 1998, New Astron. Rev., 42, 459
Ellerbroek B. L., Tyler D. W., 2001, PASP, 110, 165
Fusco T., Conan J.-M., Mugnier L. M., Michau V., Rousset G., 2000, A&AS, 142, 149
Irbah A., Chibani M., Lakhal L., Berdja A., Borgnino J., Martin F., Assus P., 2001, in Proc. SF2A-2001: Semaine de l'Astrophysique Francaise. EdP-Sciences, Paris, p. 59
Klückers V. A., Wooder N. J., Nicholls M. J., Munro I., Dainty J. C., 1998, A&AS, 130, 141
Laurant S., Deron R., Séchaud M., Rousset G., Moldij G., 1995, in Proc. OSA/ESO Topical Meeting on Adaptive Optics. ESO, Garching bei Munchen, p. 453
Le Louarn M., Hubin N., Sarazin M., Tokovinin A., 2000, MNRAS, 317, 535
Martin F., Tokovinin A., Ziad A., Conan R., Borgnino J., Avila R., Agabi A., Sarazin M., 1998, A&A, 336, L49
Sarazin M., Roddier F., 1990, A&A, 227, 294
Schöck M., Spillar E. J., 1998, Opt. Lett., 23, 150
St-Jacques D., 1998, PhD thesis, Univ. Cambridge
St-Jacques D., Cox G. C., Baldwin J. E., Mackay C. D., Waldram E. M., Wilson R. W., 1997, MNRAS, 290, 66
Vernin J., Muñoz–Tuñón C., 1994, A&A, 284, 311
Welsh B. M., 1992, Appl. Opt., 31, 7282
Wilson R. W., O'Mahoney N., Packham C., Azzaro M., 1999, MNRAS, 309, 379

This paper has been typeset from a TEX/LATEX file prepared by the author.